**Aalborg Universitet**

AALBORG UNIVERSITY

# Tunable Handset Antenna

*Enhancing Efficiency on TV White Spaces*

Barrio, Samantha Caporal Del; Foroozanfard, Ehsan; Morris, Art; Pedersen, Gert F.

*Published in:*
I E E E Transactions on Antennas and Propagation

*DOI (link to publication from Publisher):*
10.1109/TAP.2017.2662221

*Publication date:*
2017

*Document Version*
Accepted author manuscript, peer reviewed version

Link to publication from Aalborg University

*Citation for published version (APA):*
Barrio, S. C. D., Foroozanfard, E., Morris, A., & Pedersen, G. F. (2017). Tunable Handset Antenna: Enhancing Efficiency on TV White Spaces. *I E E E Transactions on Antennas and Propagation*, *65*(4), 2106 - 2111. https://doi.org/10.1109/TAP.2017.2662221

**General rights**
Copyright and moral rights for the publications made accessible in the public portal are retained by the authors and/or other copyright owners and it is a condition of accessing publications that users recognise and abide by the legal requirements associated with these rights.

- Users may download and print one copy of any publication from the public portal for the purpose of private study or research.
- You may not further distribute the material or use it for any profit-making activity or commercial gain
- You may freely distribute the URL identifying the publication in the public portal -

**Take down policy**
If you believe that this document breaches copyright please contact us at vbn@aub.aau.dk providing details, and we will remove access to the work immediately and investigate your claim.

Downloaded from vbn.aau.dk on: June 18, 2025

# IEEE TAP Communication

## Tunable Handset Antenna: Enhancing Efficiency on TV White Spaces

Samantha Caporal del Barrio, Ehsan Foroozanfard, Art Morris, and Gert F. Pedersen

***Abstract*— With the future long term evolution (LTE) auction for television white spaces at 600 MHz, there is a strong need for efficient handset antennas operating at very low frequencies. This communication shows a tunable antenna covering the LTE bands from 600 MHz to 2.6 GHz. The antenna uses state-of-the-art microelectromechanical system tunable capacitors in order to reconfigure its operating frequency. In this communication, the design mitigates the tuning loss with a tunable extended ground plane. The resulting dual-resonant antenna exhibits a peak total efficiency of −3.9 dB at 600 MHz.**

***Index Terms*— Antenna efficiency, eigenvalues and eigenfunctions, microelectromechanical devices, mobile antennas, multifrequency antennas, reconfigurable antennas.**

### I. Introduction

The ever increasing thirst for data rate leads to the standardization of the fourth generation (4G) of mobile communication, featuring long term evolution (LTE) and LTE-advanced technologies. The specifications for 4G extend the bandwidth, increase the number of antennas, and define carrier aggregation combinations, among others. The bandwidth enhancement includes bands ranging from 699 MHz to 2.690 GHz. In particular, low bands are challenging to address on a handset, given the well-known antenna design tradeoff between size, bandwidth, and efficiency [1]. The number of bands allocated to 4G keeps increasing, as a result of the spectrum release that occurred with the transition to digital television (TV), thus opening up the TV white spaces (TVWSs). The Federal Communications Commission currently holds an auction for the bands at 600 MHz [2]. These frequencies offer attractive features, such as high building penetration and wide range coverage. The work in [3] shows that the coverage is improved from 94% to 100% when using TVWS instead of legacy carriers. However, handset manufacturers are concerned about designing small antennas for such low frequencies, apprehending low antenna efficiency. This communication presents a handset antenna covering LTE bands, including the new 600-MHz bands, with very good performance.

The proposed design uses frequency reconfigurability. It is a promising technique to enable low frequency operation on small antennas. Tuning can involve different components, such as p-i-n diodes, varactor diodes, field-effect transistor, switching with variable transmission line lengths, switching with different matching circuits, switched capacitors, switches using microelectromechanical systems (MEMSs) technology, or MEMS tunable capacitors, among others. Exhaustive overviews are given in [4] and [5]. The authors choose to use MEMS tunable capacitors, in light of their low insertion loss, high-voltage handling, and very low power consumption [6]. However, tuning decreases the antenna efficiency [7]. Indeed, as the radiating element is tuned further away from the resonance of the ground plane, the unloaded quality factor ($Q$) increases, thus leading to higher currents on the board [8]. Power is dissipated through the equivalent series resistance (ESR) of the tuner, the dielectric material (e.g., Fr-4) and the copper, i.e., nonperfect electric conductor (PEC) [9].

The contribution of this communication is to efficiently address the 600-MHz bands on a handset. While the work in [10] presents the advantages of using an independently tunable dual-resonant design to cover such low bands on a handset, this communication presents a new antenna design that has no cut-back, covers the LTE high bands, and yields a higher peak efficiency. The following details the antenna principle which is here to continuously tune the ground plane resonance simultaneously with tuning the antenna element, in a dual-resonant manner. Indeed, while a typical smartphone ground plane exhibits a resonance around 1 GHz [11], [12], loading it lowers its resonance frequency [13], [14]. This communication pays a particular attention to the resonance frequency of the ground plane with the unique insight provided by the Theory of Characteristic Modes (TCM) [15]. The design focuses on preventing the unloaded antenna $Q$ from rising too rapidly with tuning, in order to mitigate loss. This communication shows how tuning the ground plane resonance to the antenna operating frequency enhances efficiency, i.e., 2 dB at 600 MHz with the proposed design.

### II. Tuning Principle

In the low bands, adjusting the chassis resonance enhances the efficiency at the operating frequency. To tune the ground plane, a metallic element—named ground plane extension (GPE)—is connected to it through an inductor. The electrical length of the ground plane varies with the value of the inductor. Simultaneously, the antenna is tuned on the feeding line. The schematics of the tunable antenna and the tunable ground plane are given in Fig. 1. The values for $L1$, $L2$, and $C_m$ are detailed in Section III-C. In practice, tunable inductors are very bulky and lossy; therefore, a high-$Q$ fixed inductor is used in parallel with an MEMS tunable capacitor for the measurements. However, for the proof of concept, the simulations are conducted with a tunable inductor. It is worth noting that simulating the tank circuit of the corresponding reactance values leads to overlapping results.

#### A. Impact of Ground Plane Loading on the Mode Behavior

The scattering electromagnetic fields of a conducting body can be changed by impedance loading [16]. To show the impact of reactive loading on the scattering fields of a large conducting body, the TCM [15], [17] is used. Consider a conducting body with a loaded surface $S$, the impressed electric field $E^i$ induces a current $J$ on $S$ and

Manuscript received October 24, 2016; accepted December 12, 2016. Date of publication February 1, 2017; date of current version April 5, 2017. This work was supported by the Danish National Advanced Technology Foundation through the project entitled Enhancing the Performance of Small Terminal Antennas With MEMS Tunable Capacitors.

S. Caporal del Barrio is with the Section of Antennas, Propagation and Radio Networking, Department of Electronic Systems, Faculty of Engineering and Science, Aalborg University, Aalborg 9220, Denmark, and also with wiSpry, Irvine, CA 92618 USA (e-mail: scdb@es.aau.dk).

E. Foroozanfard and G. F. Pedersen are with the Section of Antennas, Propagation and Radio Networking, Department of Electronic Systems, Faculty of Engineering and Science, Aalborg University, Aalborg 9220, Denmark (e-mail: gfp@es.aau.dk).

A. Morris is with wiSpry, Irvine, CA 92618 USA.

Color versions of one or more of the figures in this communication are available online at http://ieeexplore.ieee.org.

Digital Object Identifier 10.1109/TAP.2017.2662221

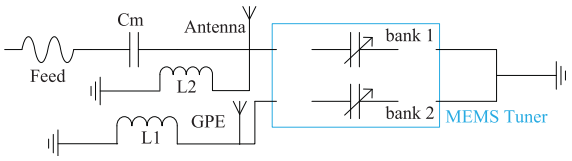


Fig. 1. Antenna and GPE tuning concept: the tank circuit combining $L2$ and bank 1 of the MEMS tunes the antenna; $L1$ and bank 2 of the MEMS tune the GPE. The fixed capacitor $C_m$ matches the antenna to the feed line. There is no connection between the feed line or the antenna and the GPE.

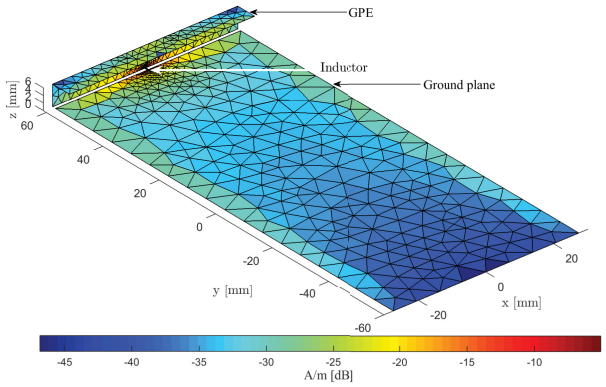


Fig. 2. Current distribution of the first resonant mode $J_1$, i.e., the dipole mode, on the ground plane and on the GPE at resonance in the low-band region.

it is related to the surface current by a linear operator $L(\cdot)$. Moreover, $[L(J) - E^i]_{\tan} = 0$, where the term $-L(J)$ gives the scattered field intensity $E$ at any point in space as a result of the induced current $J$ on $S$. The operator $L(\cdot)$ has the dimension of the total impedance matrix of the surface $S$. The notation $(Z + Z_L)(J) = [L(J)]_{\tan}$ is introduced, where $Z$ is the method of moments (MoM) matrix of the surface $S$ and $Z_L$ is the impedance matrix of the reactive load. Harrington and Mautz [18] introduce a modal solution by selecting $[L(J)]_{\tan} = (1 + i\lambda_n)R(J_n)$, which leads to

$$(X + X_L)(J_n) = \lambda_n R(J_n) \tag{1}$$

where $X$ and $X_L$ represent the imaginary part of the impedance matrix and $R$ represents the real part. The vector $\lambda_n$ is defined as the eigenvalues of the $n$th mode across frequency and its sign indicates the type of stored energy for each mode. That is to say, the mode is inductive for a positive value of $\lambda_n$ and capacitive for a negative value of $\lambda_n$. Furthermore, the resonance of each mode occurs when $\lambda_n$ equals zero.

The following considers inductive loading of the PEC ground plane with ideal loads located on each MoM basis function [19]. The diagonal entries of the load matrix are given by $X_{L,i} = wL_i e_i^2$, where $w$ is the angular frequency, $L_i$ the $i$th inductance, and $e_i$ the edge length of the $i$th element.

### B. Analysis of the Ground Plane Tuning

The aforementioned theory is applied to a 120 mm × 55 mm ground plane, connected to a GPE with no cut-back. Fig. 2 shows the current distribution of the first mode (dipole mode) on the ground plane and on the GPE at resonance. The first mode is dominant in the low bands and the current distribution is calculated by the MoM method with 1037 triangle basis functions [20]. The study of the modal behavior of the loaded GPE is conducted by placing the inductive load in an edge element located between the ground plane and the GPE. By varying the value of the inductor connecting the ground plane and the GPE, the resonance of the ground plane

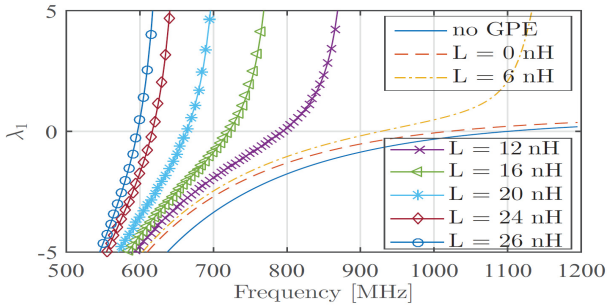


Fig. 3. Eigenvalues of the first mode ($\lambda_1$) of the tuned ground plane.

can be tuned. Fig. 3 shows the eigenvalues of the first mode ($\lambda_1$) across frequency. The ideal inductor varies from 6 to 26 nH, leading to a resonance shifting from 930 to 600 MHz. For reference, the eigenvalues of the ground plane alone (no GPE) and the unloaded GPE ($L = 0$ nH) are also plotted.

The unloaded $Q$ ($Q_{\text{unloaded}}$) refers to $Q$ when the metallic plates are modeled with PEC and the tuning is made with ideal components. It is calculated for the ground plane with a feed and an antenna according to

$$Q(\omega_0) = \frac{\omega_0 |Z'(\omega_0)|}{2R} \tag{2}$$

where $\omega_0$ is the frequency, $Z$ is the impedance and $R$ is the resistance [8]. The antenna geometry is described in Section III and detailed in Fig. 4. The calculation step size is 0.25 MHz and the first mode is largely dominant in the radiation mechanism at low frequencies. The addition of the GPE decreases $Q_{\text{unloaded}}$ of the resulting antenna from 12 to 7 at 900 MHz and from 288 to 135 at 615 MHz. That is a reduction of 42% and 53%, respectively. The significant decrease in $Q$ at the lowest tuning stage leads to the efficiency enhancement that will be seen in Sections IV-B and IV-C.

## III. Tunable Design

The proposed design shows that mobile communications are feasible on bands around 600 MHz and that the antenna can provide sufficient total efficiency. Moreover, the antenna volume is fair, as the total thickness amounts to 9.6 mm, which is in line with the most recent phones in the market [21]. No cut-back on the printed circuit board (PCB) is needed, that is an optimization of the phone dimensions to address the LTE real-estate challenge and place many amplifiers, e.g., PAs and LNAs, and many filters its bandwidth requires.

### A. Antenna and GPE Geometries

The dimensions of the antenna are shown in Fig. 4. Both radiators are identical in their geometry. The design has been patented in [22] and comprises three elements, namely, the antenna, the ground plane, and the GPE. The antenna is connected to the feeding line, whereas the GPE is not. The TCM applied to a rectangular ground plane indicates that the best location for a capacitive exciter of low frequencies is along the short edge of the ground plane, as it is the minima of the current distribution for the first eigenmode [23]. Moreover, a center feed provides maximum bandwidth potential [12]. In order to use a single tuner to tune both the antenna and the GPE and to minimize insertion loss, the antenna and the GPE are colocated. However, there is no direct connection between the antenna and the GPE. The matching and tuning components are inserted

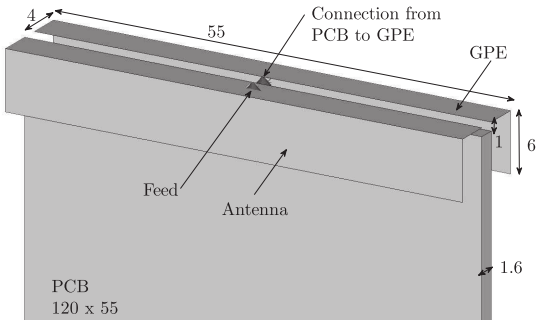


Fig. 4. Antenna and GPE geometries (dimensions in mm).

between the feeding line and the antenna, as well as between the feeding line and the GPE.

### B. MEMS Tunable Capacitor

A MEMS tunable capacitor is used on the antenna structure in order to tune it, from the bands in the GSM-900 region down to the bands in the 600-MHz region. The work uses a state-of-the-art packaged MEMS tuner from wiSpry, namely, the 1040 tuner. It comprises four high-resolution tunable capacitors, grouped into two independent banks. Its dimensions are 2.2 mm × 2.6 mm and it includes a series inductance $L_{\text{series}}$ of $4.5 \times 10^{-4}$ nH and a shunt capacitance $C_{\text{sh}}$ of 1 pF throughout the operating frequency range. These parasitics are mainly responsible for the minimum capacitance of the tuner $C_{\text{min}} = 0.5$ pF. The maximum capacitance of the whole chip is $C_{\text{max}} = 11.9$ pF and the resolution is $C_{\text{step}} = 0.125$ pF. To tune the antenna to 600 MHz, bank 1 of the tuner takes its maximum value 5.9 pF. In that case, $Q$ is 164 and the ESR is 0.3 Ω. At 850 MHz for $C_{\text{min}}$, $Q$ is 691 and the ESR is 0.5 Ω.

### C. Matching and Tuning Circuitry

Both the antenna and the GPE are tunable. The purpose of the design is to tune the ground plane resonance as the antenna is tuned. The antenna schematics can be seen in Fig. 1, where $C_m = 1.8$ pF (ESR being 0.15 Ω at 850 MHz and 0.16 Ω at 600 MHz), $L1 = 6.9$ nH (ESR being 0.28 Ω at 850 MHz and 0.23 Ω at 600 MHz), and $L2 = 5.4$ nH (ESR being 0.21 Ω at 850 MHz and 0.18 Ω at 600 MHz). The fixed inductors $L1$ and $L2$ are high-$Q$ air inductors from Coilcraft, whereas the fixed capacitor $C_m$ is a typical 0402 capacitor from Murata.

## IV. Measurements

Prototypes of the antenna design were built and tested on a network analyzer for the return loss and in the StarLab chamber from Satimo for the total efficiency ($\eta_T$).

### A. Demonstrators

Pictures of the demonstrating board are shown in Fig. 5. The antenna is soldered on the front side of the board (to PAD1) and hides the tuning network. On the back side of the board, there is no network and the GPE is soldered. $C1$–$C4$ and $C6$–$C9$ are dc supply control capacitors and are not involved with RF lines. While Fig. 5(a) shows the antenna and the GPE, Fig. 5(b) focuses on the tuning and matching components. In design B, each of the independent banks of the single 1040 tuner is connected to either the antenna or the GPE. $L1$, $U1$, $C5$, and $L2$ are part of the matching and tuning network. $C5$ corresponds to $C_m$ in Fig. 1. $L1$ is only used in design B.

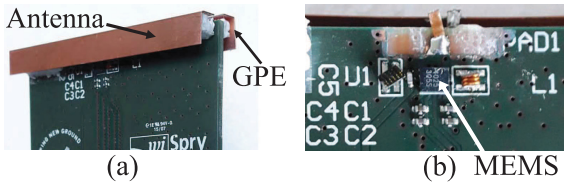


Fig. 5. Demonstrator board. (a) Demonstrator with the antenna and the GPE mounted. (b) Detailed view of the matching and tuning network for design B. The MEMS tuner ($U1$) has two independent banks, one for controlling the antenna and one for controlling the GPE.

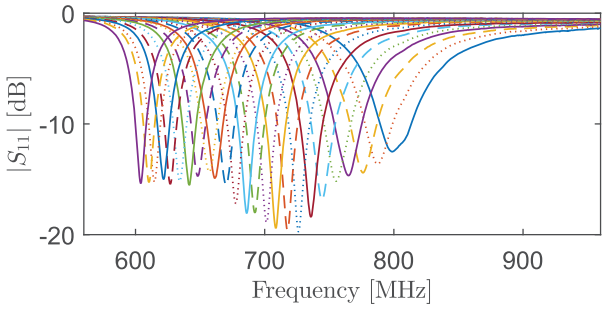


Fig. 6. Return loss of design A when the 1040 MEMS tuner varies from 0.5 to 6.5 pF in steps of 0.25 pF.

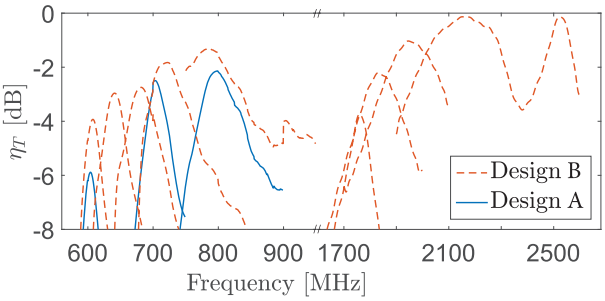


Fig. 7. Total efficiency of design A (without GPE) for minimum, medium, and maximum capacitance of the 1040 MEMS tuner in the low bands, and of design B (with GPE) when the 1040 MEMS tuner varies according to the settings described in IV-C.

### B. Design A: Reference Design

Design A is introduced as a reference, it tests the tuning of the antenna alone. $L1$ and the GPE are not mounted on the PCB. Its purpose is to evaluate, by comparison, the benefit of adding the GPE in design B. Having only the antenna mounted on the board is an example of a typical antenna tuning approach. The schematics of this design are identical to the schematics shown in Fig. 1, except for the bank 2 that is opened. Even though the MEMS has a resolution of 0.125 pF, the proposed designs only needs steps of 0.25 pF to cover all the frequencies from 850 to 600 MHz.

*1) Return Loss:* The measured return loss of design A is shown in Fig. 6. One can observe a classical single-resonance antenna being tuned over the low frequencies of the communication spectrum. The impedance bandwidth at −6 dB shrinks as the antenna is tuned. It varies from 51 MHz at the highest bound to 17 MHz at the lowest bound.

*2) Peak Efficiency:* Fig. 7 shows the measured total efficiency of the demonstrator for design A and for design B. For design A, the efficiency is only plotted for three states of the tuner: the minimum capacitance (0.5 pF), the midrange capacitance (3 pF), and the maximum capacitance (5.9 pF). For design B, all the states are

TABLE I
LOSS DECOMPOSITION FOR DESIGNS A AND B

| | Design A Loss at 600 MHz [dB] | Design B Loss at 609 MHz [dB] |
|---|---|---|
| Copper + trace + Fr-4 | 3.3 | 2.2 |
| $C_m$ = 1.8 pF | <<0.1 | <<0.1 |
| L2 = 5.4 nH | 1.9 | 1.0 |
| L1 = 6.9 nH | - | 0.7 |
| 1040 bank 1 | 1.0 | 0.3 |
| 1040 bank 2 | - | 0.4 |
| Total radiation | 6.2 | 4.6 |
| Mismatch | 0.3 | 0.1 |
| Total | 6.5 | 4.7 |

plotted. The measured peak total efficiency of design A decreases from −2.1 dB at 800 MHz to −2.5 dB at 700 MHz and to −5.9 dB at 600 MHz. The power loss is due to loss in the PCB (feeding trace, Fr-4), in the antenna (copper is not a PEC but a lossy metal), and in the ESR of the matching and tuning components (fixed components and MEMS tuner). Mismatch loss is negligible.

With the frequency solver of the Computer Simulation Technology (CST) software, the following data can be collected.

1) At 800 MHz, the thermal loss (including the trace loss, the dielectric loss, the conductor loss, and the ESR loss) is 1.3 dB. The peak total loss (including the thermal loss and the mismatch loss) is 1.6 dB.
2) At 600 MHz, the thermal loss is 6.2 dB. The ESR loss (from both the tuner and the fixed components) is 2.9 dB. Moreover, 3.3 dB of the thermal loss is due to the trace, Fr-4, and copper. The peak total loss is 6.5 dB. This loss decomposition is summarized in Table I.

The simulated and measured radiation efficiencies at 600 MHz (−6.2 and −5.9 dB, respectively) are in very good agreement. They differ by 0.3 dB, which belongs to the uncertainty of the measurement. Related work on single antenna design reports similar peak total efficiencies: −6 dB at 600 MHz in [24], −4 dB at 700 MHz [25], [26], and −2.6 dB at 750 MHz in [27]. It can be noted that the trace loss can be both simulated and measured. In both cases, the trace loss is 0.18 dB at 850 MHz and 0.15 dB at 600 MHz.

### C. Design B: Antenna and GPE

In design B, both the antenna and the GPE are mounted on the board. The MEMS tuner comprises two independent banks; bank 1 is used on the antennas and bank 2 on the GPE. In the following, five tuning states are considered, where bank 1 takes the values [0.0, 1.3, 2.8, 4.7, 5.9], while bank 2 takes the values [0.0, 0.9, 2.0, 2.9, 3.7] simultaneously.

*1) Return Loss:* Fig. 8 shows the dual-resonance resulting from the addition of the GPE to the antenna design. The antenna is responsible for one resonance and the GPE for the other one, as indicated in Fig. 8. It is worth noting that the GPE cannot be a standalone resonance, as it is not fed directly. The antenna resonance exhibits a harmonic in the high bands, which can be tuned with the same settings. The overall bandwidth at −6 dB covers LTE bands from [578–831] MHz, [1756–2312] MHz, and [2501–2586] MHz.

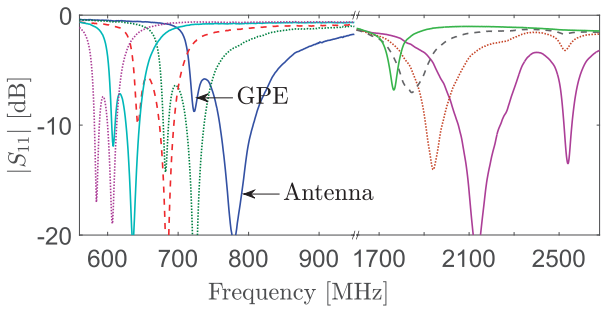


Fig. 8. Return loss of design B in the low and high bands of the LTE spectrum where the tuner varies according to the settings described in IV-C.

*2) Peak Efficiency:* The total efficiency of the demonstrator for design B is measured and shown in Fig. 7 for the low and high bands. The peak total efficiency decreases as follows: −1.4 dB at 785 MHz, −1.8 dB at 720 MHz, −2.2 dB at 684 MHz, −2.9 at 641 MHz, and −3.9 dB at 608 MHz. The mismatch loss in the low bands is negligible, since one can observe in Fig. 8 that the return loss is below −15 dB. Therefore, the total and the radiation efficiencies are indistinguishable. In the high bands, the peak total efficiencies vary from −0.5 dB at 2520 and 2000 MHz to −2.2 dB at 1800 MHz and to −3.7 dB at 1750 MHz.

In the following, we detail the contribution of each element to the total loss in the low bands. Using the simulation tool, the contribution of each component to the total loss can be isolated. It is summarized in Table I. It can be observed that the contributions of banks 1 and 2 differ, even though their ESR is identical. This is because they are connected to different elements (the antenna or the GPE). Those two elements have a different reactance and different current densities, which explains the difference in dissipated power. Moreover, the power dissipated by $L2$ differs between design A and design B, which is due to a lower $Q$ of the antenna (because the GPE is added), thus a lower current density. Similarly, the thermal loss (copper+trace+Fr-4) is decreased for design B, compared with design A. This is also due to the lower $Q$ that design B exhibits, thanks to the GPE. The total simulation loss is 4.7 dB. The simulated and measured conductor and dielectric loss at 600 MHz (−4.6 and −3.9 dB, respectively) differ by 0.7 dB, which is within the measurement accuracy.

Compared with design A, the use of the GPE enhances the peak total efficiency by 1.8 dB at 600 MHz.

*3) Efficiency Bandwidth:* The efficiency bandwidth has been defined and investigated in [28]. When real components are used, the efficiency bandwidth provides a more relevant information than the impedance bandwidth. Unfortunately, no threshold has been standardized for the measure of the efficiency bandwidth. In the following, the authors choose an efficiency threshold of −5 dB to read the efficiency bandwidth in the low bands, i.e., below 1 GHz. This value is chosen according to related work. In [29], the free space (FS) total radiated power is reported to be between 23 and 31 dBm in the GSM-900 bands for common phones in the market today, and the antenna total efficiency is calculated to average at −4 dB on those bands. The conducted measurements show an antenna total efficiency spreading from −3 to −7 dB in the GSM-900 bands. In [30], the antenna total efficiency at 700 MHz has been reported to peak at −5 dB for the main antenna and −7 dB for the secondary antenna. Therefore, a threshold of −5 dB for evaluating the efficiency bandwidth is realistic, though a tough requirement at 600 MHz. Naturally, the higher the peak efficiency, the wider

TABLE II
EFFICIENCY BANDWIDTHS [MHz] FOR THE FIVE TUNING STATES OF DESIGN B

| Low bands | | | High bands |
|---|---|---|---|
| at -5 dB | at -4 dB | at -3 dB | at -3 dB |
| 950 - 745 | 853 - 720 | 838 - 740 | 2597-2423, 2343-1949 |
| 772 - 682 | 760 - 688 | N/A | 2086 - 1839 |
| 720 - 648 | 711 - 659 | N/A | 1891 - 1785 |
| 621 - 660 | N/A | N/A | N/A |
| 618 - 598 | N/A | N/A | N/A |

the bandwidth. Moreover, as the threshold is lowered the efficiency bandwidth increases.

The efficiency bandwidths of design B are summarized in Table II. In the low bands, they vary from 205 to 20 MHz. The standard for the channel bandwidths has not been defined yet for the 600-MHz bands. However, it is known that for the 800-MHz bands, the maximum channel bandwidth is 10 MHz and the duplex spacing is 45 MHz; thus, the maximum required bandwidth is 65 MHz. Similarly, for the 700-MHz bands, the maximum channel bandwidth is 10 MHz and the duplex spacing is 30 MHz; thus, the maximum required bandwidth is 50 MHz. It can be observed that it typically decreases with frequency.

The states 4 and 5 offer an efficiency bandwidth of 40 and 20 MHz, respectively, for a threshold at $-5$ dB. The authors believe that in light of the maximum bandwidth requirements for the 800-MHz bands and the 700-MHz bands, a requirement of 40 MHz for the 600-MHz bands is realistic. Therefore, the proposed design complies down to 620 MHz. In the eventuality that state 5 would not comply, the efficiency threshold would lower for those particular frequencies in order to enhance the efficiency bandwidth. For example, the $-6$ dB efficiency bandwidth is 50 MHz for state 4. The high bands use an efficiency bandwidth threshold at $-3$ dB. The frequencies between 2343 and 2423 MHz require a threshold at $-3.5$ dB. The uplink frequencies of band 3 exhibit an efficiency between $-3$ and $-5$ dB, whereas the downlink of band 7 is limited by the minimum capacitance of the tuner.

## V. USER EFFECT

Investigations on the user effect are conducted with simulations only, using the transient solver of CST.

### A. Phone Components

The phone battery, screen glass, and plastic casing are added to the model. The relative permittivity and electrical conductivity are, respectively, 3.75 and 0.001 S/m for the screen, and 2.8 and 0.002 S/m for the casing. The battery is a grounded metallic box. At 600 MHz, the influence of the phone components in FS is limited: detuning of 1 MHz, 1% bandwidth increase and 0.2 dB additional loss.

### B. Body Loss

The head and the hands used in the following are modeled according to CTIA specifications [31]. Fig. 9(a) shows the antenna in talk mode, placed between the specific anthropomorphic mannequin (SAM) head and the talk-mode hand grip, while Fig. 9(b) shows the antenna in portrait data-mode, placed in the data-mode hand grip. In both cases, the antenna is placed in the palm of the hand. The return loss is compared between the FS and the user case in Fig. 10. At low bands, the mismatch loss is very low for both user cases. At high bands, mismatch is significant with the user's head and hand in the lowest tuning state ($C_{\max}$); and the detuning is significant with the data hand. Detuning can be compensated for, as the proposed antenna is frequency-reconfigurable. Hence, the relevant loss to investigate is the absorption loss. At 600 MHz, the simulation with the user's head and talk-mode hand yields a radiation efficiency of $-13$ dB. That is 9 dB lower than in FS. Moreover, the simulation with the user's data-mode hand shows a radiation efficiency of $-5$ dB, i.e., 1 dB lower than in FS. This values are in agreement with typical absorption loss due to the presence of the user [32].

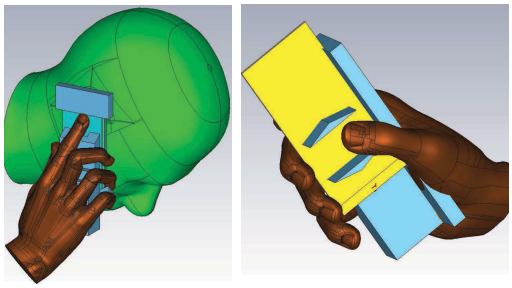

(a) (b)

Fig. 9. Antenna simulations with the user effect. In (a) with the CTIA SAM head and talk-mode hand phantoms, in (b) with the CTIA data hand phantom.

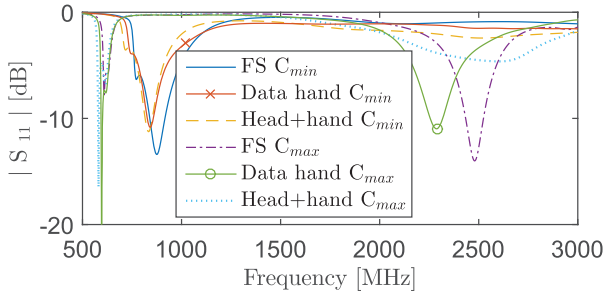


Fig. 10. Return loss in FS, in the presence of the user phantom in talk mode [Fig. 9(a)] and in the presence of the user hand in data mode [Fig. 9(b)].

### C. Specific Absorption Rate

The specific absorption rate (SAR) is a measure of the user exposure to electromagnetic radiation and should be below 1.6 W/kg over a 1-g mass of tissue [33]. In the SAR simulations, the antenna is placed at the bottom of the phone, the phone is oriented 60° to the vertical axis of the SAM and it is placed at 5 mm from the ear. Considering 23-dBm power for LTE, the SAR simulations peak at 0.4 W/kg at 600 MHz and 0.6 W/kg at 2.6 GHz. The GSM-band simulation shows a peak SAR of 0.96 W/kg at 900 MHz with 24-dBm input power. The averaging method used is IEEE C95.3 and the computed values meet the SAR guidelines for commercial phones.

## VI. CONCLUSION

This communication presents a tunable handset antenna design addressing the future bands for mobile communication at 600 MHz with MEMS tunable capacitors. Its contribution lies in the ability to excite the structure efficiently at such low frequencies. High efficiencies are obtained by continuously loading the ground plane

as the antenna is tuned. The design does not require a cut-back, which is a major advantage to manufacturers. Anechoic chamber measurements yield a peak total efficiency of $-4$ dB at 600 MHz, where using the GPE leads to a 2 dB improvement. Finally, the gain in network infrastructure resulting from a 2 dB improvement of the mobile antenna efficiency has a significant potential. Future work concerns MIMO capabilities of the proposed design.

## REFERENCES


[1] R. F. Harrington, "Effect of antenna size on gain, bandwidth, and efficiency," *J. Res. Nat. Bureau Standards*, vol. 64D, no. 1, pp. 1–12, Jan./Feb. 1960.

[2] FierceWireless. *Incentive Auction of 600 MHz Spectrum Kicks Off*, accessed on Oct. 21, 2016. [Online]. Available: http://www.fiercewireless.com/story/incentive-auction-600-mhz-spectrum-kicks/2016-03-29

[3] C. F. Silva *et al.*, "Extension of LTE operational mode over TV white spaces," in *Proc. Future Network and Mobile Summit Conf.*, Warsaw, Poland, 2011, pp. 1–13.

[4] L. Huang and P. Russer, "Electrically tunable antenna design procedure for mobile applications," *IEEE Trans. Microw. Theory Techn.*, vol. 56, no. 12, pp. 2789–2797, Dec. 2008.

[5] J. T. Bernhard, *Reconfigurable Antennas*. San Rafael, CA, USA: Morgan & Claypool, 2007.

[6] N. Haider, D. Caratelli, and A. G. Yarovoy, "Recent developments in reconfigurable and multiband antenna technology," *Int. J. Antennas Propag.*, vol. 2013, Jan. 2013, Art. no. 869170.

[7] S. C. del Barrio, A. Tatomirescu, G. F. Pedersen, and A. Morris, "Novel architecture for LTE world-phones," *IEEE Antennas Wireless Propag. Lett.*, vol. 12, pp. 1676–1679, 2013.

[8] A. D. Yaghjian and S. R. Best, "Impedance, bandwidth, and Q of antennas," *IEEE Trans. Antennas Propag.*, vol. 53, no. 4, pp. 1298–1324, Apr. 2005.

[9] S. C. del Barrio, P. Bahramzy, S. Svendsen, O. Jagielski, and G. F. Pedersen, "Thermal loss in high-Q antennas," *Electron. Lett.*, vol. 50, no. 13, pp. 917–919, Jun. 2014.

[10] S. C. del Barrio, A. Morris, and G. F. Pedersen, "MEMS tunable antennas to address LTE 600 MHz-bands," in *Proc. 9th Eur. Conf. Antennas Propag. (EuCAP)*, Apr. 2015, pp. 1–4.

[11] P. Vainikainen, J. Ollikainen, O. Kivekas, and I. Kelander, "Resonator-based analysis of the combination of mobile handset antenna and chassis," *IEEE Trans. Antennas Propag.*, vol. 50, no. 10, pp. 1433–1444, Oct. 2002.

[12] J. Villanen, J. Ollikainen, O. Kivekas, and P. Vainikainen, "Coupling element based mobile terminal antenna structures," *IEEE Trans. Antennas Propag.*, vol. 54, no. 7, pp. 2142–2153, Jul. 2006.

[13] C.-H. Chang and K.-L. Wong, "Bandwidth enhancement of internal WWAN antenna using an inductively coupled plate in the small-size mobile phone," *Microw. Opt. Technol. Lett.*, vol. 52, no. 6, pp. 1247–1253, Jun. 2010.

[14] S. Wang and Z. Du, "A dual-antenna system for LTE/WWAN/WLAN/WiMAX smartphone applications," *IEEE Antennas Wireless Propag. Lett.*, vol. 14, pp. 1443–1446, 2015.

[15] R. F. Harrington and J. R. Mautz, "Theory of characteristic modes for conducting bodies," *IEEE Trans. Antennas Propag.*, vol. 19, no. 5, pp. 622–628, Sep. 1971.

[16] J. K. Schindler, R. B. Mack, and P. Blacksmith, "The control of electromagnetic scattering by impedance loading," *Proc. IEEE*, vol. 53, no. 8, pp. 993–1004, Aug. 1965.

[17] R. J. Garbacz and R. Turpin, "A generalized expansion for radiated and scattered fields," *IEEE Trans. Antennas Propag.*, vol. 19, no. 3, pp. 348–358, May 1971.

[18] R. Harrington and J. Mautz, "Control of radar scattering by reactive loading," *IEEE Trans. Antennas Propag.*, vol. 20, no. 4, pp. 446–454, Jul. 1972.

[19] E. Safin and D. Manteuffel, "Manipulation of characteristic wave modes by impedance loading," *IEEE Trans. Antennas Propag.*, vol. 63, no. 4, pp. 1756–1764, Apr. 2015.

[20] S. Makarov, *Antenna and EM Modeling With MATLAB*. Hoboken, NJ, USA: Wiley, 2002.

[21] *2015 Smartphone Comparison Guide*, accessed on Feb. 2016. [Online]. Available: http://www.gizmag.com/2015-smartphone-comparison-guide-1/36992/

[22] S. C. del Barrio, A. Morris, and G. F. Pedersen, "Patent: Tunable dual-resonance antenna for handsets operating in low LTE bands with wide duplex spacing," U.S. Patent 62 065 106, Oct. 2014.

[23] R. Martens, E. Safin, and D. Manteuffel, "Inductive and capacitive excitation of the characteristic modes of small terminals," in *Proc. Antennas Propag. Conf. (LAPC)*, Loughborough, U.K., Nov. 2011, pp. 1–4.

[24] Y. Chen, R. Martens, R. Valkonen, and D. Manteuffel, "Evaluation of adaptive impedance tuning for reducing the form factor of handset antennas," *IEEE Trans. Antennas Propag.*, vol. 63, no. 2, pp. 703–710, Feb. 2015.

[25] A. Singh *et al.*, "Compact active antenna for mobile devices supporting 4G LTE," in *Proc. Loughborough Antennas Propag. Conf. (LAPC)*, Nov. 2014, pp. 525–529.

[26] L. H. Trinh *et al.*, "Reconfigurable antenna for future spectrum reallocations in 5G communications," *IEEE Antennas Wireless Propag. Lett.*, vol. 15, pp. 1297–1300, Dec. 2015.

[27] S. W. Lee, H. S. Jung, and Y. J. Sung, "A reconfigurable antenna for LTE/WWAN mobile handset applications," *IEEE Antennas Wireless Propag. Lett.*, vol. 14, pp. 48–51, 2015.

[28] J. Rahola and R. Valkonen, "Using the concept of obtainable efficiency bandwidth to study tunable matching circuits," in *Proc. 6th Eur. Conf. Antennas Propag.*, Mar. 2012, pp. 1869–1872.

[29] A. Tatomirescu and G. F. Pedersen, "User body loss study for popular smartphones," in *Proc. Eur. Conf. Antennas Propag.*, Apr. 2015, pp. 1–4.

[30] S. C. del Barrio and G. F. Pedersen, "Correlation evaluation on small LTE handsets," in *Proc. Veh. Technol. Conf.*, Sep. 2012, pp. 1–4.

[31] "CTIA certification: Test plan for wireless device over-the-air performance revision 3.4.2," CTIA, San Francisco, CA, USA, Tech. Rep., May 2015.

[32] M. Pelosi, O. Franek, M. B. Knudsen, M. Christensen, and G. F. Pedersen, "A grip study for talk and data modes in mobile phones," *IEEE Trans. Antennas Propag.*, vol. 57, no. 4, pp. 856–865, Apr. 2009.

[33] *IEEE Standard for Safety Levels With Respect to Human Exposure to Radio Frequency Electromagnetic Fields, 3 kHz to 300 GHz*, ANSI/IEEE Standard C95.1-2005, IEEE Standards Coordinating Committee Standard, 2006.